Journal of Marine Research, 58, 297–325, 2000

On the influence of bottom topography and the Deep Western Boundary Current on Gulf Stream separation

by Claire E. Tansley[1] and David P. Marshall[1]

ABSTRACT

The Gulf Stream separates abruptly from the North American coastline at Cape Hatteras. The absence of significant seasonal and interannual variability in the separation point, compared with that of other separating boundary currents, suggests that Gulf Stream separation is locally controlled. In this paper we consider the possible influence of bottom topography and the Deep Western Boundary Current (DWBC), which descends underneath the Gulf Stream at Cape Hatteras.

The path of the DWBC is strongly constrained by bottom topography. At Cape Hatteras, the continental shelf widens and the DWBC is forced to swing offshore and pass beneath the Gulf Stream. Three possible mechanisms by which bottom topography and the DWBC can affect the separation of the Gulf Stream are proposed and investigated: (i) topography modifies the background potential vorticity contours; (ii) the DWBC "advects" the Gulf Stream separation point southward; (iii) intense downwelling as the DWBC passes beneath the Gulf Stream induces an adverse pressure gradient in the Gulf Stream, leading to its separation.

Results from a series of idealized numerical experiments with a "geostrophic vorticity" model are presented to investigate these mechanisms. Topography alone does have an impact on the separation point, broadly consistent with modification of the background potential vorticity. We also show that the presence of a DWBC does, indeed, push the time average separation of the Gulf Stream farther southward, consistent with both the advection and adverse pressure gradient mechanisms. However, the time-dependent boundary current separation is more nonlinear than suggested by each of the above mechanisms, undergoing a series of abrupt transitions between northern and southern separation states. As the DWBC transport is increased, the southern separation state is occupied more and more frequently.

1. Introduction

The Gulf Stream follows the North American coastline northward until it reaches Cape Hatteras, at which point the Gulf Stream abruptly separates and strikes out into the North Atlantic. A remarkable aspect of Gulf Stream separation, and one that must be explained by any theory of Gulf Stream separation, is the intransience of the separation latitude. Auer (1987) has provided a comprehensive description of the Gulf Stream path over a five year period dating from June 1980 to June 1985. The annual-mean and seasonal-mean paths, defined here as the location of the landward surface edge, are reproduced in Figure 1 and

1. Department of Meteorology, University of Reading, Reading RG6 6BB, United Kingdom. ***email: d.p.marshall@reading.ac.uk***

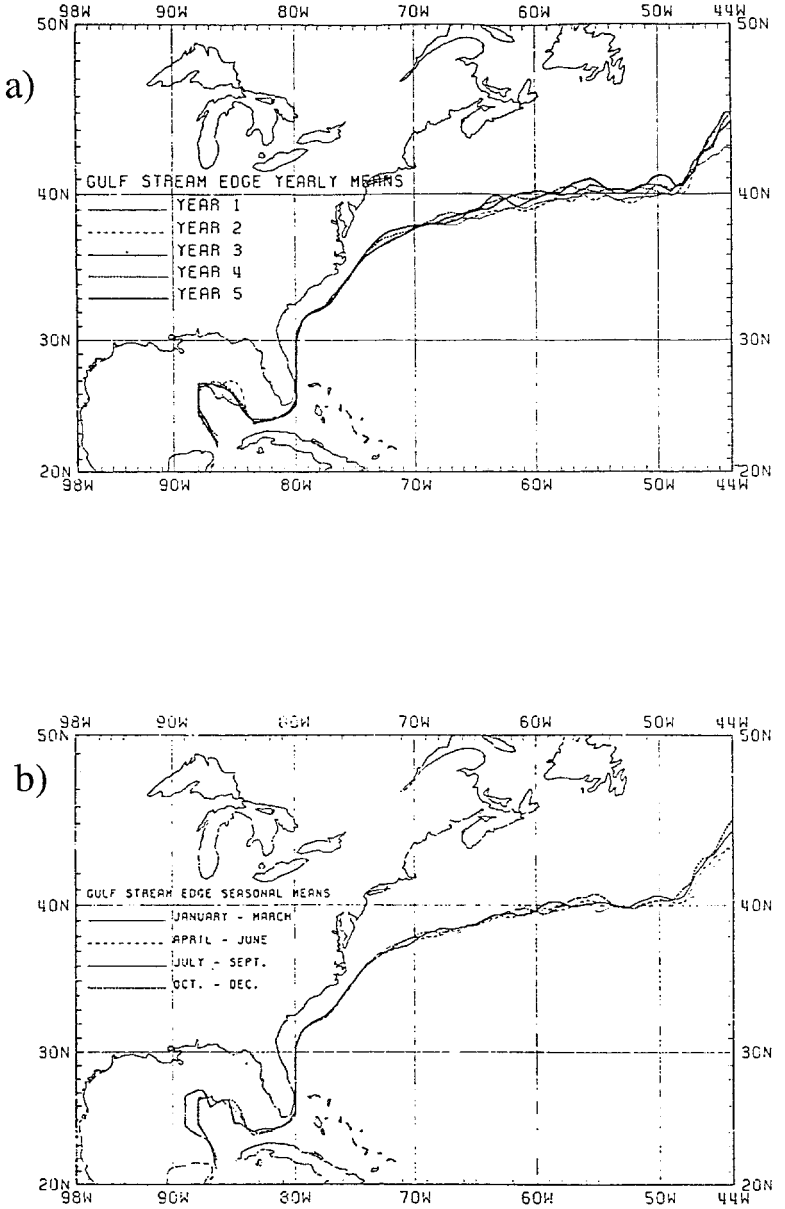

Figure 1. Position of the landward edge of the Gulf Stream inferred from satellite sea-surface temperature observations (Auer, 1987). (a) Annual mean paths over 5 years (1980–1985); (b) seasonal mean paths over the five years. Note the remarkable absence of variability in the separation latitude.

reveal little interannual or seasonal variability. This is in marked contrast to the separation behavior of other western boundary currents, for example the along-coast ranges of separation for the Brazil Current and Malvinas Current are 930 km and 850 km, respectively (Olson *et al.,* 1988).

A number of mechanisms have been proposed to explain Gulf Stream separation. These include the line of zero wind-stress curl, outcropping of the main thermocline (Parsons, 1969; Veronis, 1973), separation by vorticity crisis (Cessi *et al.,* 1990), and maintenance of a northern recirculation gyre by buoyancy forcing (Ezer and Mellor, 1992). Dengg *et al.* (1996) provide a comprehensive review. Large-scale wind and buoyancy forcing, together with eastern boundary processes, must play a role in determining the path of the Gulf Stream. However, the absence of significant variability suggests that the exact position of the Gulf Stream separation point is locally controlled. There are two key factors that might provide this local control: coastline geometry, and interactions with the Deep Western Boundary Current (DWBC) and bottom topography.

The coastline turns sharply northward at Cape Hatteras; thus it is tempting to argue that the coastline separates from the Gulf Stream. Stern and Whitehead (1990) showed in both numerical and laboratory experiments that for a fixed barotropic jet profile, separation occurs at an obtuse-angled boundary, provided the angle exceeds a critical value. Using a barotropic ocean model with idealized coastline geometries, Dengg (1993) was, in certain cases, able to obtain separation. However Dengg's experiments exhibit sensitivity to the choice of lateral boundary condition and the strength of the wind forcing. Özgökmen *et al.* (1997) extended Dengg's study to include baroclinicity and idealized topography and obtained broadly similar results.

In this paper, we consider the influence of the DWBC and bottom topography on Gulf Stream separation. A steep continental shelf follows the coast of North America; this alone must have important implications for the vorticity budget of the Gulf Stream. The DWBC is formed at high latitudes and flows southward along the continental shelf, as sketched in Figure 2. At Cape Hatteras, the continental shelf abruptly widens, forcing the DWBC to swing offshore and underneath the Gulf Stream. Observations (Pickart and Watts, 1990; Pickart and Smethie, 1993; Bower and Hunt, 2000) suggest that the DWBC descends approximately 800 m as it passes under the Gulf Stream. This localized descent implies a localized stretching of vortex tubes in the Gulf Stream above.

While previous numerical studies by Thompson and Schmitz (1989) and Spall (1996a,b) have considered the impact of the DWBC on the Gulf Stream, surprisingly little attention has been given to the widening of the continental shelf, which controls the point at which the Gulf Stream and DWBC must intersect. The aim of this paper is to investigate the influence of both the DWBC and the geometry of the continental shelf on the separation of the Gulf Stream. In the spirit of Dengg (1993), who considered only the effects of irregular coastlines, in this paper we exclude irregular coastlines to isolate the effects of shelf geometry and the DWBC.

In Section 2, we introduce three mechanisms by which the topography and the DWBC

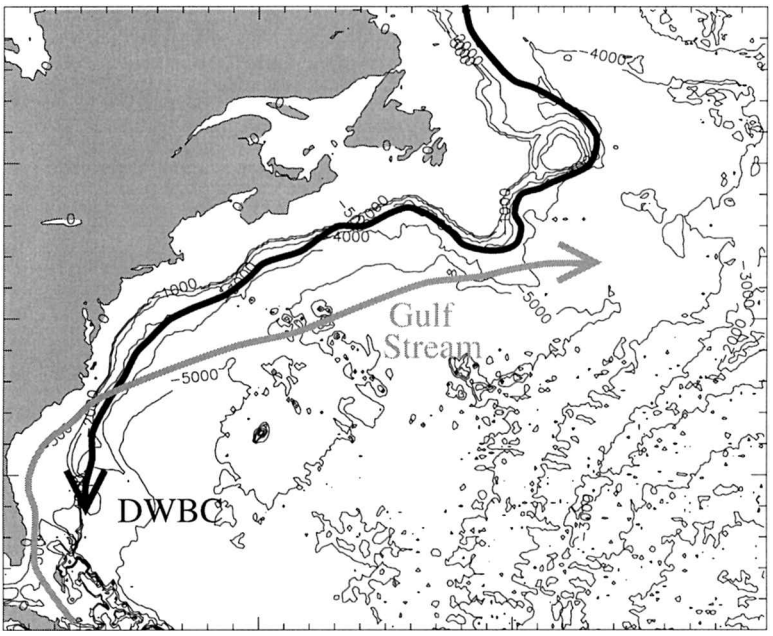

Figure 2. The paths of the Gulf Stream and the DWBC. Contours show bottom topography. Contour interval is 1000 m; the 500 m contour is also shown. Note how the DWBC swings offshore at Cape Hatteras where the continental shelf widens.

might influence the separation of the Gulf Stream. In Section 3, we motivate and describe the formulation of a numerical "geostrophic vorticity model." In Section 4, we present results from a series of idealized two-layer numerical experiments, containing a DWBC flowing along a continental shelf in the lower layer, and wind-driven subtropical and subpolar gyres in the upper layer. Finally, in Section 5, we discuss the wider implications of our results for the observed separation, and for numerical ocean models.

2. Separation mechanisms

In this section, we describe three mechanisms by which topography and the DWBC might influence the path of the Gulf Stream. The first two mechanisms—modification of the background potential vorticity field by topography, and southward advection of the separation point by the DWBC—have been previously proposed. The third mechanism involves a new analysis of the vorticity budget at the separation point, and demonstrates that the DWBC can induce an adverse pressure gradient in the Gulf Stream, and hence its separation.

a. Modification of background potential vorticity by topography

The primary influence of variable bottom topography on Gulf Stream separation is likely to be through modification of the background potential vorticity field. Using linear

planetary-geostrophic dynamics, Salmon (1992, 1994) obtained solutions for a two-layer ocean above an idealized, straight continental shelf along the western boundary. He found a tendency for the circulation to reorientate itself southwest-northeast along the background potential vorticity contours, leading to a southward shift of the separation point of the upper layer boundary current, compared to the case without topography. However, it is not clear that these results carry over to the more realistic scenario in which nonlinear accelerations are included. For example, Thompson (1995) included continental rises at the boundaries of a quasi-geostrophic model, but found this gave no change in the separation point. Furthermore, Özgökmen *et al.* (1997) showed that in some cases, flow along potential vorticity contours with the addition of topography led to their model Gulf Stream separating too far north, but as the strength of the boundary current increased, its inertia enabled it to cross background potential vorticity contours and separate correctly at an idealized coastal promontory, representing Cape Hatteras.

A precise examination of the potential vorticity balance at the Gulf Stream separation point requires knowledge of not just the Coriolis parameter and topography distributions, but also the stratification. An alternative approach is to consider the "joint effects of baroclinicity and relief" (JEBAR) on the Gulf Stream. This approach has been used to diagnose the effects of baroclinicity and topography from climatological data (e.g., Greatbatch *et al.,* 1991; Myers *et al.,* 1996) and model data (Bell, 1999). The JEBAR forcing generally leads to a southward shift in the Gulf Stream separation latitude in these diagnostic studies. However there is a real danger of confusing cause and effect with the JEBAR approach, since the Gulf Stream separation at Cape Hatteras is imprinted on the observed density field, and hence on the diagnosed JEBAR forcing. In reality, the density field is free to evolve and adjust to the topographic forcing.

b. Southward "advection" of the separation point

There are two mechanisms by which the DWBC might *locally* influence the path of the Gulf Stream. In order to simplify the conceptual and mathematical analysis, both of these mechanisms will be developed in the context of a simple two-layer model. The upper layer of thickness h_1 and velocity $\mathbf{u}_1$ represents the Gulf Stream, and the lower layer of thickness h_2 and velocity $\mathbf{u}_2$ represents the DWBC; the total ocean depth is H. We exclude diapycnal fluxes between the layers due to entrainment and mixing. We imagine a situation in which there is initially no DWBC and the Gulf Stream separates to the north of Cape Hatteras. If a DWBC is suddenly introduced, then this will perturb the separation of the Gulf Stream.

Following Thompson and Schmitz (1989), the continuity equation for the upper layer can be written

$$\begin{aligned}\frac{\partial h_1}{\partial t} &= -h_1 \nabla \cdot \mathbf{u}_1 - \mathbf{u}_1 \cdot \nabla h_1 \\ &= -w_i - \mathbf{u}_1 \cdot \nabla h_1,\end{aligned} \tag{1}$$

where w_i is the vertical velocity immediately above the interface separating the two layers. Thompson and Schmitz assumed the flow is in geostrophic balance at leading order, and hence $\mathbf{u}_1 \cdot \nabla h_1 \approx \mathbf{u}_{1g} \cdot \nabla h_1 = \mathbf{u}_{2g} \cdot \nabla h_1 \approx \mathbf{u}_2 \cdot \nabla h_1$ (a form of the Margules relation; strictly this approximation relies on the ageostrophic velocity being small relative to the geostrophic velocity component *perpendicular* to the interface height contours). Thus Eq. (1) can be rewritten:

$$\frac{\partial h_1}{\partial t} \approx -w_i - \mathbf{u}_2 \cdot \nabla h_1. \tag{2}$$

The final term on the right-hand side of (2) represents an "advection" of the upper layer thickness by the lower layer velocity, i.e., a southward advection of the Gulf Stream layer by the DWBC. Thompson and Schmitz assumed that w_i is negligible, in which case the separation point migrates southward at a speed $\mathbf{u}_2$. In reality, there is likely to be some vertical descent of the DWBC under the Gulf Stream, reducing the efficiency of this advection mechanism. Nevertheless, the general tendency should still be for a southward migration of separation latitude.

The Thompson and Schmitz mechanism is inherently transient in nature, describing a theory for the southward migration of the separation point, rather than for the final steady state. However, we note that there *is* a natural limit to this southward migration, set by the geometry of the coastal shelf. South of Cape Hatteras, the continental shelf widens and the DWBC swings offshore. For the DWBC to continue equatorward, it must descend underneath the Gulf Stream, as sketched schematically in Figure 3. At this point, there should be a steady state balance in which the southward advection of the upper layer thickness by the DWBC is balanced by the downward vertical motion of the DWBC beneath the Gulf Stream, that is

$$w_i \approx -\mathbf{u}_2 \cdot \nabla h_1. \tag{3}$$

Alternatively, perhaps no steady state balance is possible, in which case the separation latitude may return abruptly northward.

c. Separation by adverse pressure gradient

In classical fluid dynamics, boundary layer separation is associated with "the empirical fact that a steady state of the boundary layer adjoining a solid boundary is impossible with an appreciable fall in the velocity of the external stream" (Batchelor, 1967). In the context of the Gulf Stream, this implies that a local deceleration of the boundary current can lead to its separation. Through Bernoulli's theorem, this is equivalent to the boundary current encountering an "adverse pressure gradient." A number of authors have proposed the generation of an adverse pressure gradient as a likely Gulf Stream separation mechanism (e.g., Haidvogel *et al.,* 1992; Baines and Hughes, 1996). Here we present new analysis of the vorticity balances within the DWBC and Gulf Stream, which shows that the DWBC indeed acts to induce an adverse pressure gradient within the Gulf Stream layer at the point where the two currents intersect.

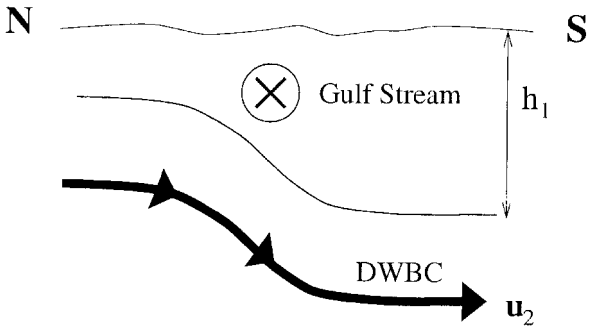

Figure 3. At Cape Hatteras, the continental shelf widens and the DWBC swings offshore. The upper layer (of thickness h_1) deepens to the south, associated with the intense eastward flow of the separated Gulf Stream (through thermal wind balance). For the DWBC (velocity $\mathbf{u}_2$) to continue southward, it must descend underneath this Gulf Stream layer as shown.

Defining a DWBC width, l, which is determined by topographic considerations rather than inertial or frictional effects, and a DWBC velocity v_2, the Rossby number for the DWBC is $Ro = v_2/fl$. Taking $v_2 \sim 0.1$ m s^{-1}, $l \sim 10^5$ m, $f \sim 10^{-4}$ s^{-1}, we obtain $Ro \sim 10^{-2}$, suggesting that relative vorticity can be neglected. This is broadly consistent with the estimates of Pickart and Smethie (1993), who find that relative vorticity is at maximum 5% of the Coriolis parameter in both the upper and lower cores of the DWBC. Thus, at leading order, assuming geostrophic balance, the vorticity budget for the DWBC can be written

$$w_i \approx w_b + \frac{\beta v_2 h_2}{f} \tag{4}$$

where w_i is the vertical velocity at the interface between the two layers and $w_b = -\mathbf{u}_2 \cdot \nabla H$ is the vertical velocity at the sea floor. Eq. (4) is equivalent to material conservation of large-scale potential vorticity, f/h_2, in the lower layer. Since this potential vorticity is dominated by variations in the bottom topography, over most of its path (4) implies that the DWBC must follow topographic contours.

At Cape Hatteras the continental shelf widens abruptly, forcing the DWBC to swing offshore. Hogg and Stommel (1985) proposed that the DWBC must slide down the continental slope in order to conserve its potential vorticity. Observational evidence of this descent was found by Pickart and Watts (1990) and Bower and Hunt (2000). Assuming a typical DWBC velocity of 10 cm s^{-1}, a descent of 800 m (Hogg and Stommel, 1985), an impact angle of 15°, and a Gulf Stream width of 100 km gives a typical vertical velocity at the crossover point of $w_b \sim -0.2$ mms^{-1}. At the crossover point, $\beta v_2 h_2/f$ is negative, and thus from (4),

$$|w_i| > |w_b|. \tag{5}$$

That is, given descent in the lower core of the DWBC, there must be even stronger vertical descent at the base of the Gulf Stream. Provided that the Rossby number remains

small, this result will carry over to a continuously stratified model, in which the upper core of the DWBC is entrained into the Gulf Stream (Pickart and Smethie, 1993).

Now turning to the Gulf Stream, what is the impact of negative w_i on the pressure distribution within the upper layer? To simplify the mathematics, we assume that the Gulf Stream flows northward (i.e., $v_1 \gg u_1$). Within the Gulf Stream layer it is essential to retain inertial accelerations. The steady-state momentum equation for the upper layer is thus

$$\mathbf{u}_1 \cdot \nabla \mathbf{u}_1 + f\mathbf{k} \times \mathbf{u}_1 + \frac{\nabla p_1}{\rho_0} = 0. \tag{6}$$

Taking the curl of (6) gives

$$\nabla \times (\mathbf{u}_1 \cdot \nabla \mathbf{u}_1) = -\frac{f w_i}{h_1} - \beta v_1, \tag{7}$$

where we have used $\nabla \cdot \mathbf{u}_1 = w_i/h_1$. At leading order, for a narrow, northward-flowing jet of minimal curvature,[2] (7) can be rewritten

$$\frac{\partial^2}{\partial x \partial y}\left(\frac{v_1^2}{2}\right) \approx -\frac{f w_i}{h_1} - \beta v_1. \tag{8}$$

Integrating (8) across the jet between an arbitrary point, x, and its outside edge, $x = \delta$ where v_1 vanishes, we find:

$$\frac{\partial}{\partial y}\left(\frac{v_1^2}{2}\right) \approx \int_x^\delta \left(\beta v_1 + \frac{f w_i}{h_1}\right) dx. \tag{9}$$

Since $w_i < 0$, the effect of vortex stretching within the boundary current is therefore to decelerate the boundary current, precisely as is required for separation in classical fluid dynamics. Conversely the β-effect accelerates the boundary current, keeping it attached to the coastline.

Taking the scalar product of velocity with the inviscid, unforced momentum equation gives,

$$\frac{D}{Dt}\left(\frac{\mathbf{u} \cdot \mathbf{u}}{2}\right) = -\mathbf{u} \cdot \frac{\nabla p}{\rho_0}. \tag{10}$$

Thus the deceleration of the boundary layer is equivalent to fluid parcels encountering an adverse pressure gradient.

In seeking to test the adverse pressure gradient mechanism, it is extremely difficult to isolate cause and effect; separation by definition implies a decrease in velocity along the

2. It is straightforward to extend the analysis to a boundary current separating from a coastline of arbitrary inclination. The β in Eq. (9) is then replaced by $\beta \cos \alpha$ where α is the orientation of the coastline relative to the north-south axis.

coastline, and by Bernoulli's principle an adverse pressure gradient. Nevertheless it should be possible to look for intense localized downwelling where the DWBC and Gulf Stream intersect as an indicator of the mechanism.

3. Geostrophic vorticity model

To test the dynamical ideas presented in the preceding section, we have developed a "geostrophic vorticity" ocean model. The model is based on the "geostrophic vorticity equations" (Schär and Davies, 1988; Allen *et al.,* 1990), which are in turn closely related to the semigeostrophic equations widely used in atmospheric studies of frontogenesis (e.g., Hoskins, 1975). In contrast to a quasi-geostrophic model, the geostrophic vorticity equations allow finite variations in bottom topography, and finite variations in isopycnal layer thickness. Vertical motion is entirely implicit, so we avoid the problems of representing vortex stretching inherent in z-coordinate primitive equation models (e.g., see Bell, 1999). Moreover, because the model is based on solution of a Rossby wave vorticity equation, it is ideally suited to studying the vorticity interactions between the Gulf Stream, DWBC and bottom topography.

We consider an idealized rectangular domain, of dimensions $L \times 2L$, with sponge layers of meridional extent L appended to the northern and southern boundaries (Fig. 4). All our experiments employ two constant density layers; the upper layer is initially 800 m, and the total ocean depth without topography is 4 km. While in reality the Gulf Stream and DWBC are composed of various water masses (Pickart and Smethie, 1993), the observations of Bower and Hunt (2000) suggest that the Gulf Stream/DWBC dynamics are reasonably described by a two-layer representation.

a. *Momentum equations*

The momentum equations are written:

$$\frac{\partial \mathbf{u}_{g^1}}{\partial t} + (f + \zeta_{g^1})\mathbf{k} \times \mathbf{u}_1 + \nabla B_{g^1} = \frac{\tau_{sx}}{\rho_0 h_1} - K\nabla^4 \mathbf{u}_{g^1} + S_1, \tag{11}$$

$$\frac{\partial \mathbf{u}_{g^2}}{\partial t} + (f + \zeta_{g^2})\mathbf{k} \times \mathbf{u}_2 + \nabla B_{g^2} = -K\nabla^4 \mathbf{u}_{g^2} - r\mathbf{u}_{g^2} + S_2. \tag{12}$$

Here $\mathbf{u}_n$ is the full (geostrophic plus ageostrophic) velocity, $\mathbf{u}_{gn} = \mathbf{k} \times \nabla p_n/\rho_0 f$ is the geostrophic velocity, $\zeta_{gn} = \partial_x v_{gn} - \partial_y u_{gn}$ is the geostrophic relative vorticity, $B_{gn} = (u_{gn}^2 + v_{gn}^2)/2 + p_n/\rho_0$ is the geostrophic Bernoulli potential, $f = f_0 + \beta y$ is the Coriolis parameter, and ρ_0 is a reference density.

The model is driven by a surface wind stress applied to the upper layer:

$$\tau_{sx} = \tau_0 \cos\left(\frac{\pi y}{L}\right) \qquad -L \leq y \leq L. \tag{13}$$

Table 1. Model parameters.

Parameter	Symbol	Value
Longitudinal extent	L	960 km
Latitudinal extent	$2L$	1920 km
Horizontal resolution	$\Delta x, \Delta y$	15 km
Timestep	Δt	5400 s
Top layer	h_1	initially 800 m
Bottom layer	h_2	initially 3200 m without topography
Coriolis parameter	f_0	$8 \times 10^{-5}\text{s}^{-1}$ at midbasin
Beta parameter	β	$2 \times 10^{-11}\ \text{m}^{-1}\text{s}^{-1}$
Surface wind stress	τ_0	$0.2\ \text{Nm}^{-2}$ (layer 1 only)
Reduced gravity	g'	$0.01\ \text{m s}^{-2}$
Reference density	ρ_0	$1035\ \text{kg m}^{-3}$
Bottom friction coefficient	r	$1 \times 10^{-7}\text{s}^{-1}$ (layer 2 only)
Biharmonic dissipation coefficient	K	$9.0 \times 10^{10}\ \text{m}^4\ \text{s}^{-1}$
Sponge layer timescale	$s(y)$	2 days (maximum)

Biharmonic diffusion is applied to both layers and a linear bottom drag applied to layer 2 only. Details of model parameters are given in Table 1.

Inflows and outflows are handled by relaxing the geostrophic velocities toward prescribed values within two sponge layers to the north and south of the domain:

$$S_1 = s(y)(\mathbf{u}_{g^{01}} - \mathbf{u}_{g^1}), \tag{14}$$

$$S_2 = s(y)(\mathbf{u}_{g^{02}} - \mathbf{u}_{g^2}), \tag{15}$$

where $s(y)$ varies with latitude as shown in Figure 4. In layer 1 we have $\mathbf{u}_{g01} = 0$, and in layer 2, $\mathbf{u}_{g02} = v_{g02}$. The velocity profiles (Fig. 4) are determined using a prescribed hyperbolic profile for the pressure, which is then used to calculate the velocity from geostrophic balance. In practice, however, the inflow and outflows only cover a few gridpoints; we have tested the sensitivity to these profiles, and the results are qualitatively robust.

b. Continuity equation

The continuity equations involve the full velocity:

$$\frac{\partial h_1}{\partial t} + \nabla \cdot (h_1 \mathbf{u}_1) = 0, \tag{16}$$

$$\frac{\partial h_2}{\partial t} + \nabla \cdot (h_2 \mathbf{u}_2) = 0, \tag{17}$$

where h_n is the thickness of each model layer.

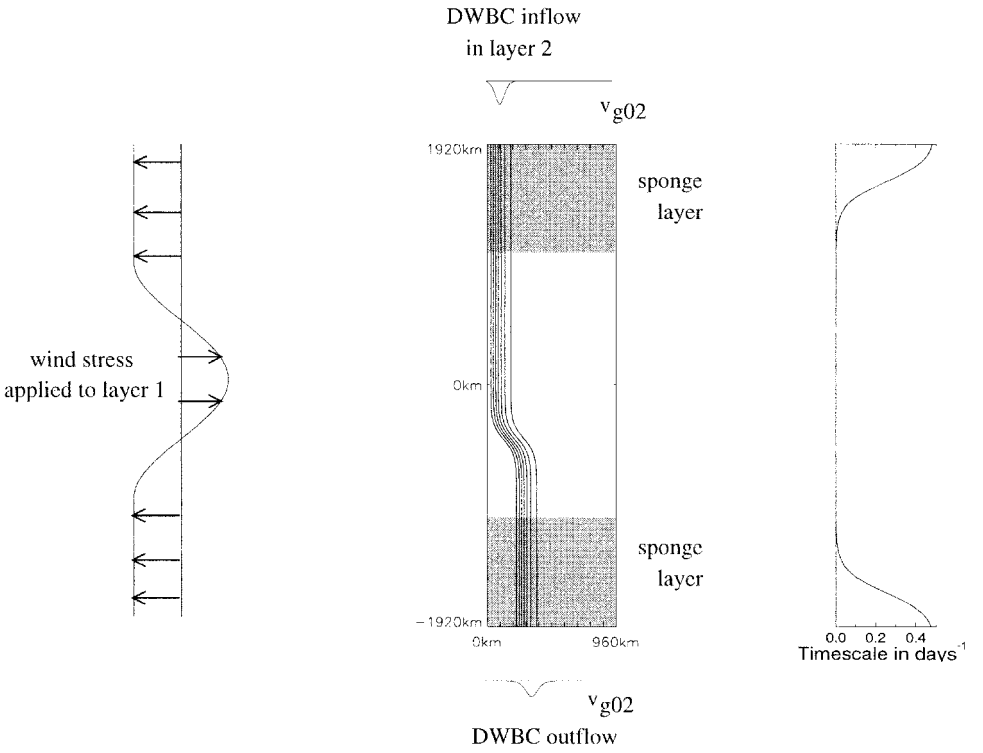

Figure 4. Model domain with an idealized continental shelf. Contours show basin depth; contour interval is 250 m. The sponge layers are denoted by shading; the right-hand panel shows the relaxation timescale.

c. Hydrostatic balance

The pressures in each layer are related through hydrostatic balance,

$$p_1 = p_2 + \rho_0 g' h_1, \tag{18}$$

where $g' = g(\rho_2 - \rho_1)/\rho_0$ is reduced gravity. A rigid lid is applied so that

$$h_1 + h_2 = H, \tag{19}$$

where H is the ocean depth. Finite variations in bottom topography are allowed provided that the Rossby number remains small in the resultant currents. Figure 5 shows the different idealized continental shelves used in our experiments.

d. Lateral boundary conditions

At solid walls, the lateral boundary condition is no-normal flow:

$$\mathbf{u}_\perp = 0. \tag{20}$$

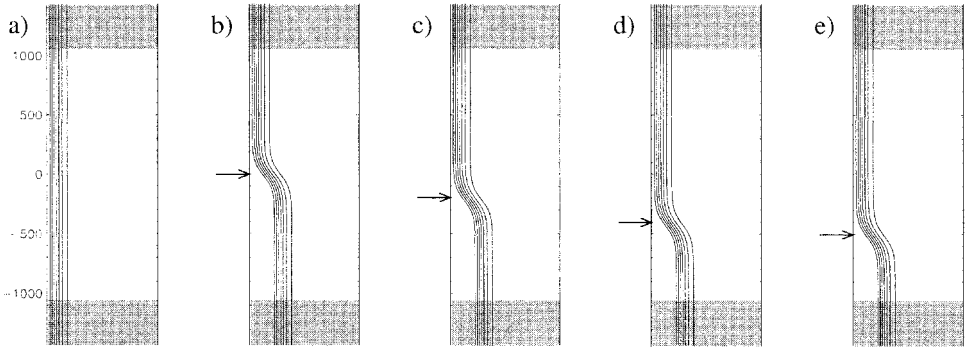

Figure 5. Bottom topography for the different experiments described in Section 4. (a) Straight shelf, (b) shelf widening near mid-basin, (c) shelf widening 200 km to south, (d) shelf widening 400 km to south, (e) shelf widening 500 km to south. Contour interval is 250 m. The arrow denotes the shelf widening point, taken as the middle of the curve in the shelf. Note that as in subsequent plots, only part of the sponge layer is shown.

The normal velocities are set to the prescribed relaxation velocities:

$$\mathbf{u}_\perp = \mathbf{u}_{g^0}, \tag{21}$$

at inflow and outflow points within the sponge layers (as detailed in Section 3a and sketched in Fig. 4).

We also apply a no-slip condition to the geostrophic velocity,

$$\nabla_\perp p = 0, \tag{22}$$

together with a similar higher order boundary condition for the biharmonic dissipation:

$$\nabla_\perp(\nabla^2 p) = 0. \tag{23}$$

e. Conservation properties

The equations lead to a material conservation relation for the geostrophic potential vorticity in each layer,

$$\frac{D}{Dt}\left(\frac{f+\zeta_{gn}}{h_n}\right) = \frac{1}{h_n}\mathbf{k}\cdot\nabla\times(\mathscr{F}_n). \tag{24}$$

Here $D/Dt \equiv \partial/\partial t + \mathbf{u}\cdot\nabla$ is the material derivative following the *full* velocity, and $\mathscr{F}_n$ represents forcing and dissipation terms on the right-hand side of (11) and (12).

The energy equation can be written:

$$\frac{\partial E}{\partial t} + \nabla\cdot\left(\sum_n B_{gn} h_n \mathbf{u}_n\right) = \sum_n h_n \mathbf{u}_n \cdot \mathscr{F}_n - \sum_n h_n \mathbf{u}_{agn}\cdot\frac{\partial \mathbf{u}_{gn}}{\partial t} \tag{25}$$

where $E = \Sigma_n h_n \mathbf{u}_{gn} \cdot \mathbf{u}_{gn}/2 + g' h_1^2/2$, and $\mathbf{u}_{ag}$ is the ageostrophic velocity. The first term on the right-hand side of (25) represents energy input through mechanical forcing; the second term arises as a result of the Geostrophic Vorticity approximation. Thus there is no exact conservation of global energy in a Geostrophic Vorticity model. However, in our integrations the last term on the right-hand side of (25) is several orders of magnitude smaller than the forcing term, and hence is of no significance.

f. Method of solution

The geostrophic vorticity equations are solved by substituting **u** from the momentum equations into the continuity equations. This gives a Rossby wave equation that can be written in the form:

$$\mathscr{L}\left(\frac{\partial p}{\partial t}\right) = \mathscr{R}, \tag{26}$$

where $\mathscr{L}$ is a known three-dimensional elliptic operator. Eq. (26) is inverted for $\partial p/\partial t$ using a three-dimensional elliptic inverter, from which p can be deducted at the forward time-step. Further details of the model grid and solution method are given in the Appendix. This formulation avoids the transformation to geostrophic coordinates used in the semigeostrophic model (Hoskins, 1975), which can be numerically unstable adjacent to coastlines (Cloke and Cullen, 1994).

4. Numerical experiments

We now present a series of experiments using our geostrophic vorticity model to explore the three mechanisms, outlined in Section 2, by which the topography and the DWBC might influence the separation of the Gulf Stream. In particular we wish to assess whether a steady separation can be maintained at the point where the continental shelf widens and the DWBC swings offshore. Rather than give a detailed account of the large number of experiments that have been performed, the following discussion focusses on a small subset of these experiments which capture the main results.

a. Control case with no topography

Firstly we consider a flat-bottomed experiment with only wind forcing, but no DWBC; the ocean depth is a uniform 4 km. We integrate for 3000 days from a state of rest.

Figure 6 shows the Bernoulli potential averaged over the last 1000 days in the two layers. The Bernoulli potential represents, to good approximation, streamlines for the flow. The upper layer shows two gyres, separated by a Gulf-Stream like jet, which leaves the western boundary mid-basin, at the line of zero wind-stress curl, in accord with classical wind-driven theory (e.g. Pedlosky, 1996). The Sverdrup transport in each gyre is approximately 30 Sv. In the lower layer a series of recirculation gyres are set up against the western boundary.

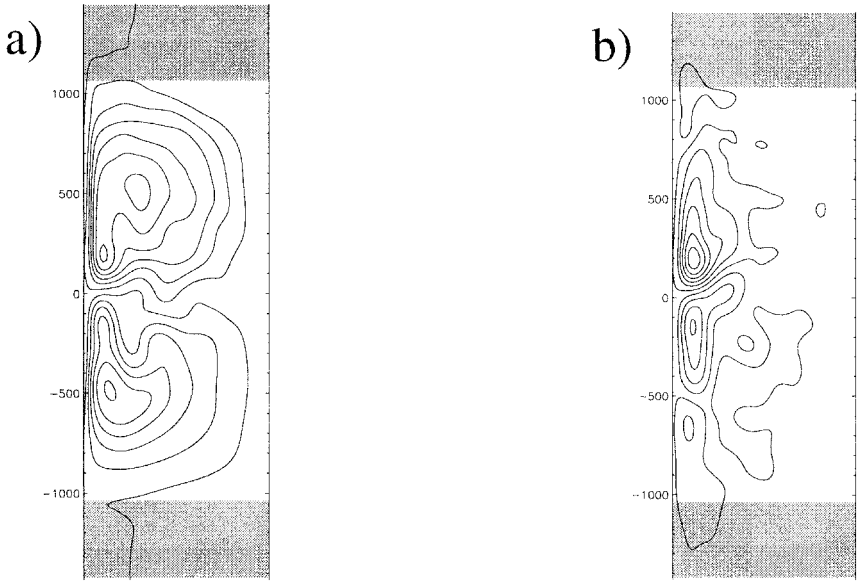

Figure 6. Time averaged Bernoulli potential in (a) the upper layer and (b) the lower layer for a control experiment with no topography or DWBC. Contour intervals are 0.4 $m^2\ s^{-2}$ for the upper layer and 0.1 $m^2\ s^{-2}$ for the lower layer.

However, there is significant variability in the separation point. In Figure 7 we show the zonal velocity component averaged over the three interior velocity points nearest to the western boundary (i.e. between $x = 15$ km and $x = 45$ km), as a function of latitude and time. The large positive values around mid-basin provide a good indication of the separation point. Periodically eddies form near the western boundary and travel toward the intergyre boundary, and the separation point is ambiguous—this shows a good resemblance to the no-slip solutions found by Haidvogel *et al.* (1992).

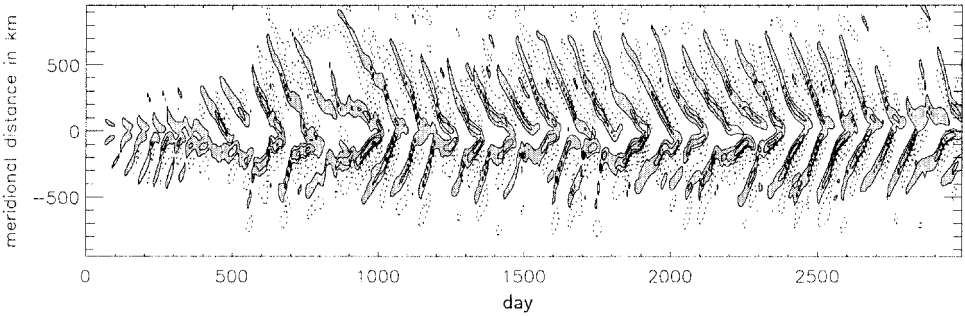

Figure 7. Time series of the zonal velocity in the upper layer, averaged between $x = 15$ km and $x = 45$ km, plotted as a function of y, for the control run. Positive contours are solid; negative contours are dotted. Contour interval is 10 cm s^{-1} (contour values are ± 5 cm s^{-1}, ± 15 cm s^{-1}, etc.). Values greater than 5 cm s^{-1}, which give a good indication of jet separation, are shaded.

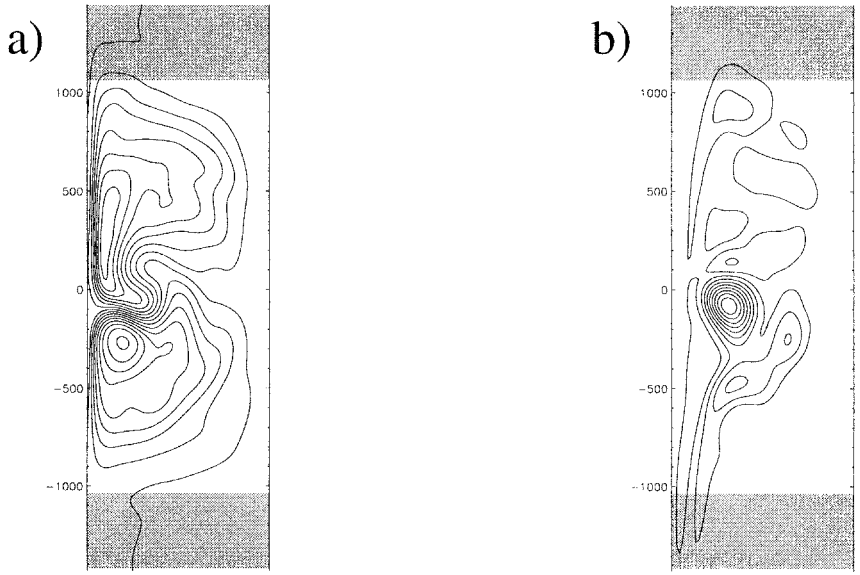

Figure 8. Time averaged Bernoulli potential in (a) the upper layer and (b) the lower layer for an experiment with a straight continental shelf. Contour intervals are 0.4 $m^2\ s^{-2}$ for the upper layer and 0.1 $m^2\ s^{-2}$ for the lower layer.

b. Influence of topography

We now introduce a 2 km high idealized continental shelf into the basin at the western boundary. This is either straight, as in previous idealized studies, or widens in the south of the basin, as in Figure 5, representing the widening of the continental shelf in the North Atlantic at Cape Hatteras. Figure 8 shows the influence of a straight continental shelf. There is a southward shift of the time average separation point in the upper layer by approximately 100 km. This is what we might expect from the topography modifying the background potential vorticity, following the results of Salmon (1992, 1994). The recirculation gyres in the lower layer are pushed away from the western boundary, and the separated boundary current is deflected northward. Figure 9 shows the influence of a continental shelf which widens 400 km to the south of mid-basin ($y = 0$), before a DWBC is included. In the lower layer, the recirculation gyres are again pushed away from the boundary, although where the shelf widens, an intense barotropic gyre forms on the shallower plateau. There is again a southward shift in the time average separation point of 100 km.

Now focusing on the time dependent behavior, Figure 10 shows time series of the separation points for experiments with a straight continental shelf, a shelf which widens mid-basin, a shelf which widens 200 km to the south and a shelf which widens 400 km to the south. On the introduction of the straight continental shelf, much of the variability seen in the control case disappears, and the separation is rather persistent (Fig. 10a). A shelf widening mid-basin introduces a very large degree of asymmetry into the basin, and the

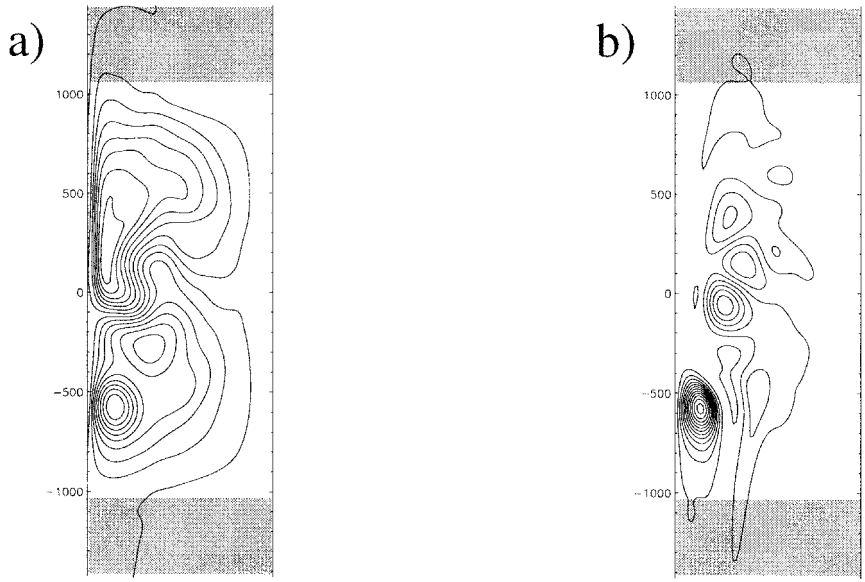

Figure 9. Time averaged Bernoulli potential in (a) the upper layer and (b) the lower layer for an experiment with a continental shelf which widens 400 km south of mid-basin. Contour intervals are 0.4 $m^2\ s^{-2}$ for the upper layer and 0.1 $m^2\ s^{-2}$ for the lower layer.

separation is nearly always to the south, resulting in a time average separation point that is 250 km to the south. If the shelf widening point is 200 km south, the southern gyre separates where the shelf widens and the northern gyre separates just 100 km south of mid-basin, as in the straight shelf case. If the shelf widening is even farther south, both gyres may separate just south of mid-basin, as in the straight shelf case, but the subtropical gyre separates at the shelf widening point for periods of a few hundred days, introducing an interesting low frequency variability. Hence the topography alone can have a dramatic influence on the separation. This is in contrast to earlier results from quasi-geostrophic models (e.g. Thompson, 1995), in which only shallow topographic slopes are permitted, and the topography has little effect on the separation point. The geometry of the shelf appears to be crucial.

Low frequency variability has been found in many other simple models. For example, Jiang *et al.* (1995) found either steady, periodic or aperiodic behavior of the separation point, depending on the asymmetry of the wind forcing and the nonlinearity of the governing equations. McCalpin and Haidvogel (1996) described the flow in their quasi-geostrophic model by infrequent and irregular transitions between a number of preferred quasi-steady states. The character of this low frequency variability was shown to be very sensitive to the model parameters; in particular, the magnitude and asymmetry of the wind forcing. The above results suggest that a continental shelf can also excite low frequency variability.

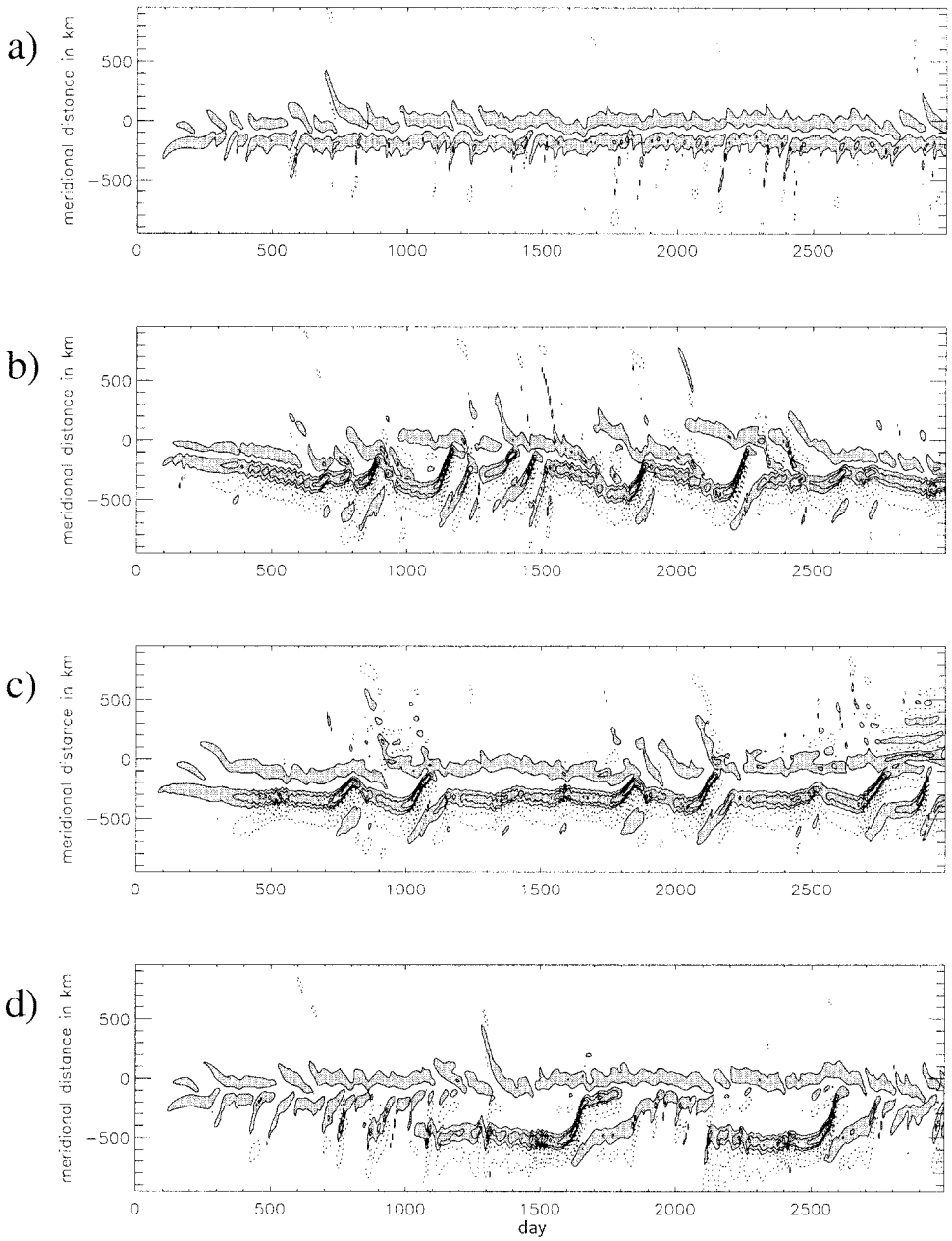

Figure 10. Time series of the zonal velocity in the upper layer, averaged between $x = 15$ km and $x = 45$ km, plotted as a function of y. Positive contours are solid; negative contours are dotted. Experiments have (a) a straight continental shelf, (b) continental shelf widening mid-basin, (c) shelf widening 200 km south of mid-basin, (d) shelf widening 400 km to the south. Contour interval is 10 cm s^{-1}; values greater than 5 cm s^{-1}, which give a good indication of jet separation, are shaded.

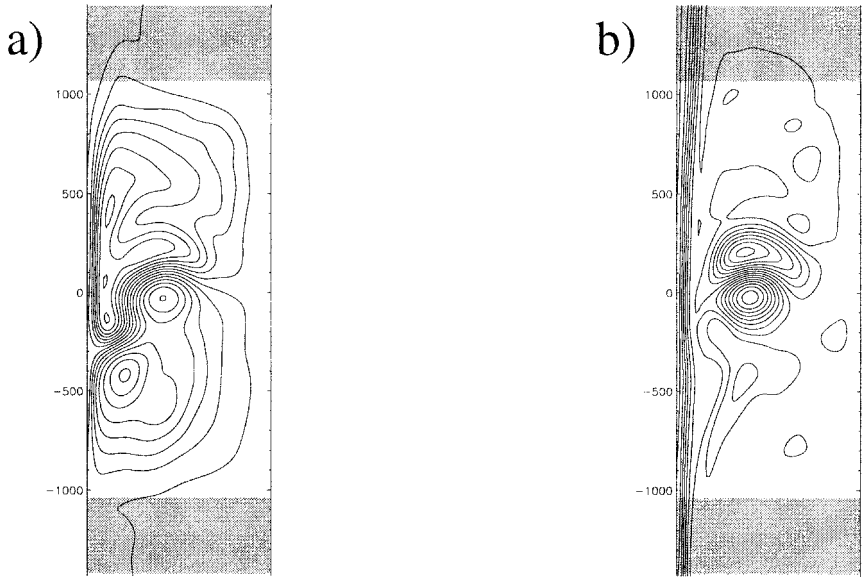

Figure 11. Time averaged Bernoulli potential in (a) the upper layer and (b) the lower layer for an experiment with a straight continental shelf and a 15 Sv DWBC. Contour intervals are 0.4 $m^2\ s^{-2}$ for the upper layer and 0.1 $m^2\ s^{-2}$ for the lower layer.

c. Sensitivity to DWBC transport with a straight continental shelf

We now introduce a DWBC of varying strengths in the lower layer by relaxing to prescribed velocities within the sponge layers as described in Section 3. First we consider the case of the straight continental shelf. Figure 11 shows the time averaged flow in both layers for a 15 Sv DWBC. The DWBC follows the continental shelf closely, as predicted in Section 2c, and consistent with the observed path of the lower core of the DWBC (Hogg and Stommel, 1985; Bower and Hunt, 2000). In common with previous studies (e.g. Thompson and Schmitz, 1989; Spall, 1996a; Ladd and Thompson, 1998), the introduction of the DWBC leads to a southward shift in the time averaged separation point. In this case there is a shift of 200 km, so that the time average separation is now 300 km south of mid-basin. If we interpret the southward shift as an 'advection' of the separation point, as described by Thompson and Schmitz (1989), we might expect the distance of the southward shift to be proportional to the strength of the DWBC. However, Eq. 9, showing the deceleration of a boundary current due to the vortex stretching induced by the DWBC, is nonlinear. We have conducted several experiments with different DWBC strengths, and find that the relationship between the southward displacement of the separation point and the DWBC transport does appear to be linear in our model, but only if a suitably long time average is taken. In addition to the variability caused by eddies, as the DWBC transport increases the separation point may become unsteady and the southern gyre separates prematurely at random intervals in the model integration.

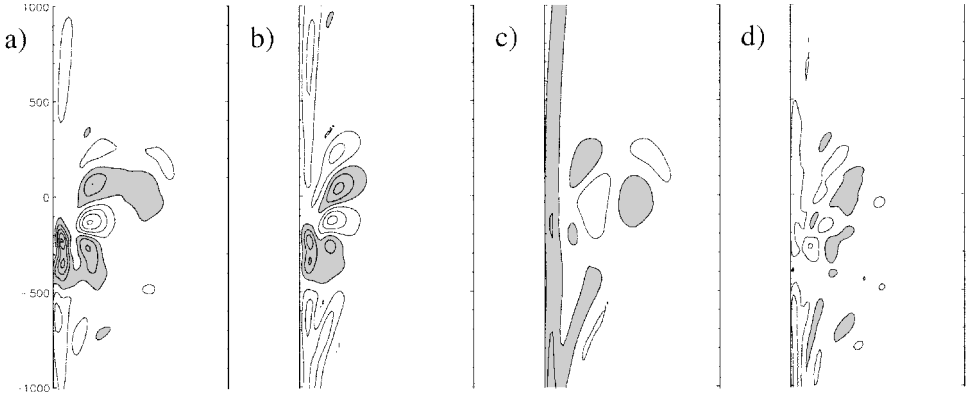

Figure 12. Components of the vorticity budget for the lower layer, Eq. (4), for the 15 Sv DWBC, straight shelf experiment. (a) Time averaged vertical velocity at the interface, w_i, (b) time averaged vertical velocity at the bottom, w_b, (c) planetary vorticity advection, $\beta v_2 h_2/f$, (d) residual, $w_i - w_b - \beta v_2 h_2/f$. Contour interval is 0.04 mm s^{-1} (contour values are $\pm$0.02 mm s^{-1}, $\pm$0.06 mm s^{-1}, etc.). Values less than $-$0.02 mm s^{-1} are shaded. The sponge layers are not shown.

As found in observations, the DWBC descends sharply as it passes beneath the upper level Gulf Stream jet. Figure 12 shows the various terms in the vorticity equation for the DWBC (Eq. 4): the vertical velocities at the layer interface and the bottom, w_i and w_b, the planetary vorticity advection, $\beta v_2 h_2/f$, and the residual. The maximum downwelling at the bottom (indicated by the shading in Fig. 12b) is about 0.14 mm s^{-1}, in line with our estimate in Section 2c. Away from the intergyre boundary, the DWBC moves upslope, in order to conserve its potential vorticity, and as found in the inverse study of Bogden *et al.* (1993). The maximum downwelling at the interface (indicated by the shading in Fig. 12a) is 0.2 mm s^{-1}. The vortex stretching in the lower layer, $w_i - w_b$, is largely balanced by the planetary vorticity advection, $\beta v_2 h_2/f$, while the residual is mainly due to the biharmonic dissipation term. In the south of the basin, the DWBC hugs the western boundary and dissipation starts to dominate the vorticity balance. This does not happen in experiments where the continental shelf widens, and the DWBC flows away from the western boundary (see next section). In the quasi-geostrophic model of Ladd and Thompson (1998) the DWBC is frictionally controlled all along the western boundary. This is probably because the continental slope is small in their model, as required for quasi-geostrophic dynamics, so that the DWBC cannot adjust its potential vorticity by traveling upslope as it travels southward.

The vortex stretching in the Gulf Stream supplied by this large vertical velocity at the interface is associated with a deceleration in the upper layer (Eq. 9). However, since separation is always accompanied by deceleration of the flow and an adverse pressure gradient, it is difficult to separate cause and effect in this case.

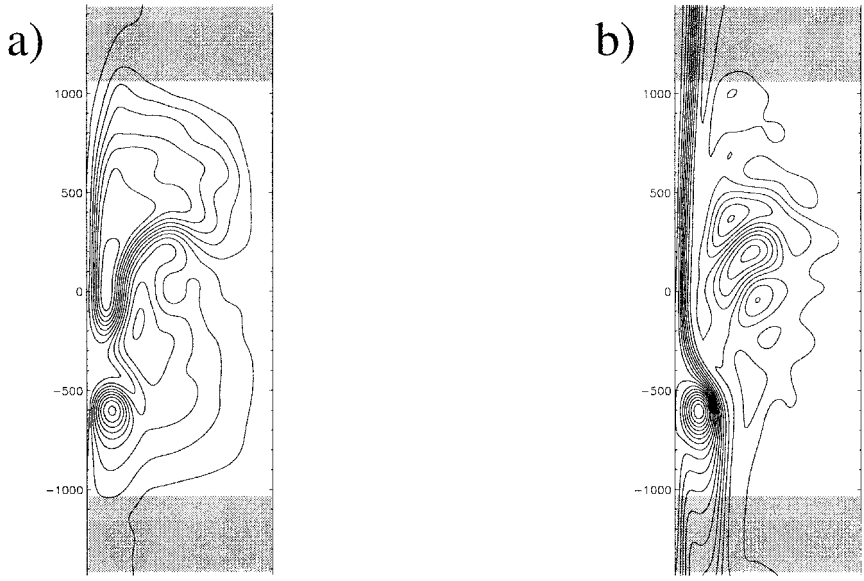

Figure 13. Time averaged Bernoulli potential in (a) the upper layer and (b) the lower layer for an experiment with a continental shelf widening 400 km south of mid-basin and a 20 Sv DWBC. Contour intervals are 0.4 $m^2\ s^{-2}$ for the upper layer and 0.1 $m^2\ s^{-2}$ for the lower layer.

d. Sensitivity to DWBC transport with a widening continental shelf

Next we examine the effect of the widening of the continental shelf. The DWBC again follows the continental shelf closely. For example, Figure 13b shows the time averaged Bernoulli potential in the lower layer for a 20 Sv DWBC, where in this case the continental shelf widens 400 km to the south. The DWBC swings offshore as the shelf widens. For this experiment there is a clear separation of the subtropical gyre in the upper layer (Fig. 13a) at the point where the shelf widens. The northern gyre separates 250 km to the south of mid-basin.

Figure 14 shows the time evolution of the separation points for experiments in which the continental shelf widens 400 km to the south, and the DWBC transport is varied. As the DWBC transport increases, the southern gyre starts to separate prematurely more and more often. For 15 Sv and 20 Sv DWBCs the two distinct separation points of the northern and southern gyres become clear throughout, and there is also reduced variability in the separation point of the subtropical boundary current. In part this may be due to the shielding of the subtropical boundary current from the subpolar boundary current, as indeed occurs in reality.

e. Sensitivity to shelf geometry with fixed DWBC transport

We now examine the effect of changing the latitude at which the shelf widens. We keep the DWBC transport fixed at 15 Sv. Figure 15 shows the time series of the separation points

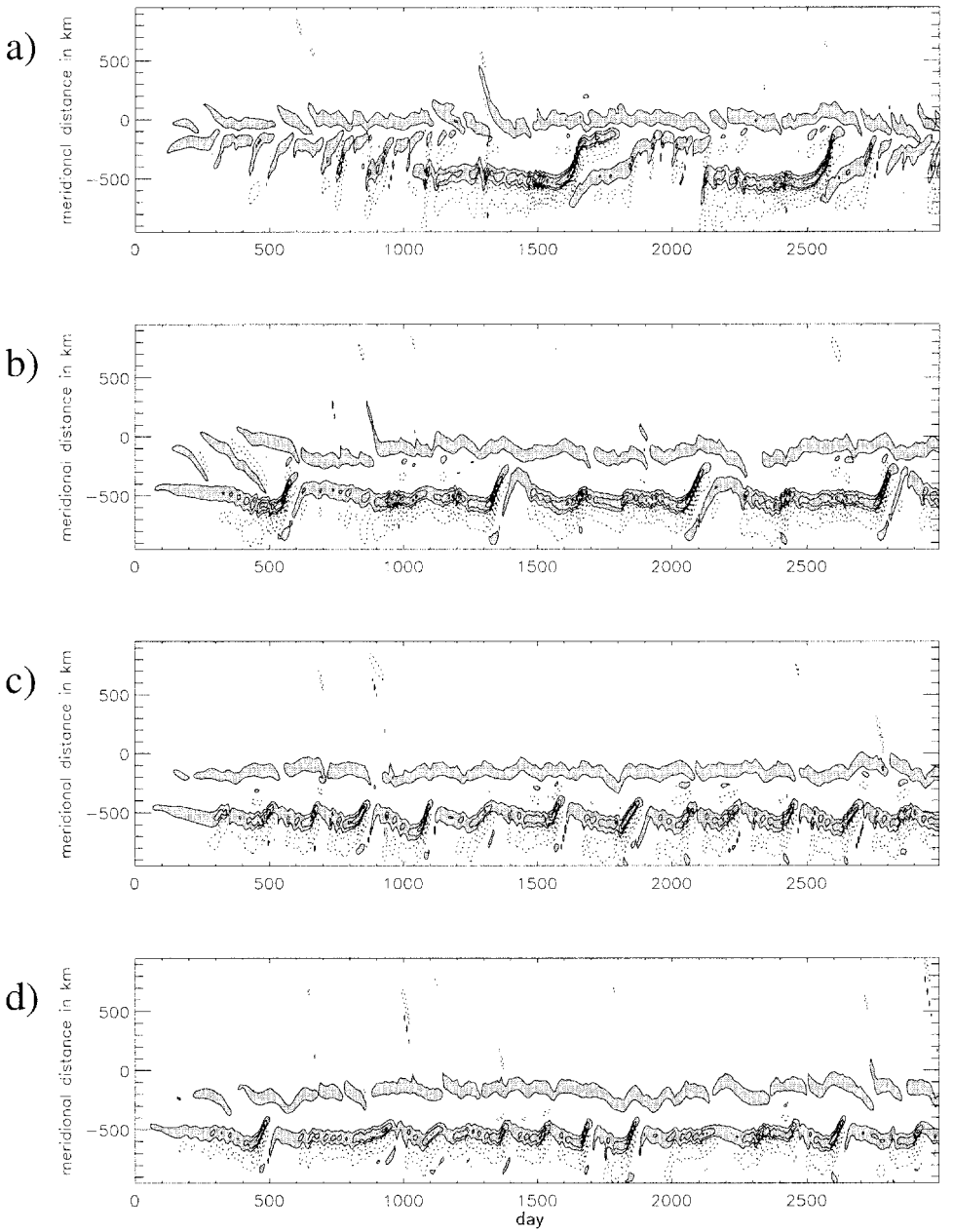

Figure 14. Time series of the zonal velocity in the upper layer, averaged between $x = 15$ km and $x = 45$ km, plotted as a function of y. Positive contours are solid; negative contours are dotted. Experiments have a continental shelf widening 400 km south of mid-basin, and different DWBC transports. (a) No DWBC, (b) 10 Sv, (c) 15 Sv and (d) 20 Sv DWBC transports. Contour interval is 10 cm s^{-1}; values greater than 5 cm s^{-1}, which give a good indication of jet separation, are shaded.

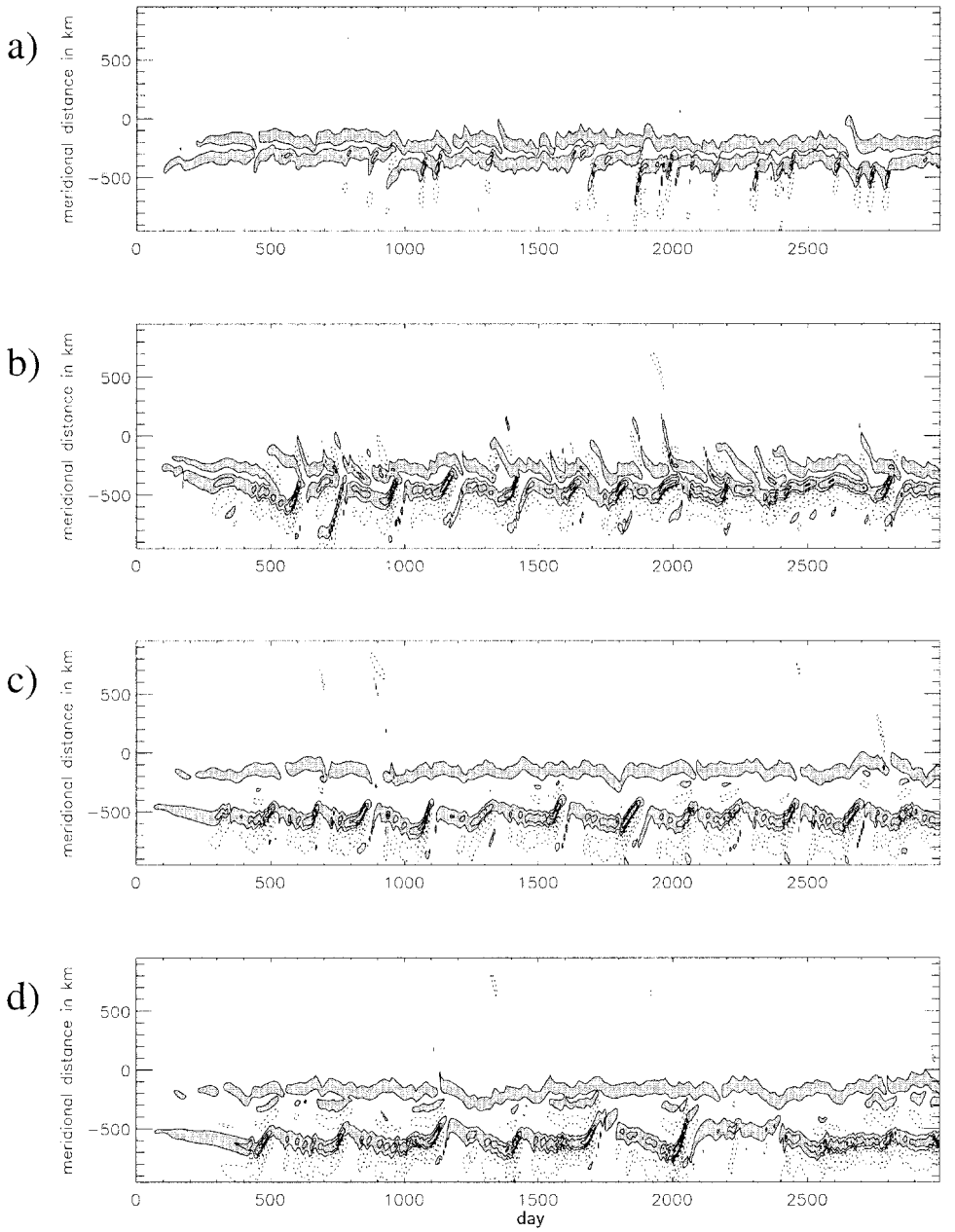

Figure 15. Time series of the zonal velocity in the upper layer, averaged between $x = 15$ km and $x = 45$ km, plotted as a function of y. Positive contours are solid; negative contours are dotted. Experiments include a 15 Sv DWBC, and a continental shelf widening at different latitudes. (a) Straight shelf, (b) shelf widening mid-basin, (c) shelf widening 400 km to the south, (d) shelf widening 500 km to the south. Contour interval is 10 cm s^{-1}; values greater than 5 cm s^{-1}, which give a good indication of jet separation, are shaded.

for some of these experiments. If the continental shelf widens at the midpoint, the time average separation occurs about 350 km to the south. The time average separation is also 350 km to the south for a shelf which widens 200 km to the south or 300 km to the south. Hence the introduction of the DWBC seems to push the separation southward despite the widening of the shelf. Examination of the lower-layer pressure field shows that the DWBC ascends the shelf where it widens in these experiments, until it reaches the Gulf Stream. As shown earlier, for a straight shelf, separation occurs 300 km to the south with a 15 Sv DWBC. So perhaps a steady separation at the shelf widening point is not possible in these cases.

However, if the shelf widens 400 km to the south or 500 km to the south, we again find two distinct separation points. The southern gyre always separates prematurely, and the separation is fairly steady. The position is determined by the widening of the continental shelf, consistent with both the advection and the adverse pressure gradient separation mechanisms. This is in contrast to the case without a DWBC, where the separation returns north after periods of a few hundred days. The separation of the northern gyre generally occurs at the same position as found in the equivalent straight shelf experiment.

f. Sensitivity to resolution and model parameters

A large number of model parameters, both physical and numerical, have an influence on the circulation patterns we find in the model. Small changes in any one of these parameters can lead to a transition to a different model regime. This is a characteristic feature of nonlinear wind driven gyres, and has been investigated in some detail by Jiang *et al.* (1995) and Berloff and Meacham (1998). However, the broad pattern of results described above does appear to be robust to variations in model parameters. For example, we have repeated the above experiments at a lower resolution of 30 km, and obtain broadly similar results (not shown).

5. Discussion

a. Role of the DWBC

A number of factors may influence Gulf Stream separation. In this paper, we have isolated the impact of the DWBC, together with the geometry of the continental shelf. Our results suggest that these alone cannot account for the observed intransience of the Gulf Stream separation, although there is clear evidence of the topography and the DWBC influencing the separation in our experiments, consistent with previous studies, including Özgökmen *et al.* (1997), Thompson and Schmitz (1989) and Spall (1996a,b).

Our theoretical analysis suggests that if the Gulf Stream initially separates north of Cape Hatteras, the DWBC may advect the separation point southward (as suggested by Thompson and Schmitz) until it reaches Cape Hatteras, where the continental shelf widens and the DWBC swings offshore. A steady state balance may be possible at this point, where the DWBC descends beneath the Gulf Stream. Formal analysis of steady state vorticity

balances suggests that the DWBC decelerates the Gulf Stream above and induces an adverse pressure gradient. However, it is difficult to prove cause and effect; the separation of the boundary current is always accompanied by an adverse pressure gradient. Haidvogel *et al.* (1992) inferred that this means separation is *caused* by an adverse pressure gradient; however we do not believe that this necessarily follows.

Numerical experiments with an idealized, straight continental shelf along the western boundary show that the topography alone can shift the time average boundary current separation point, while introduction of the DWBC provides a further southward shift, in common with previous studies. However, the situation becomes more complicated with a widening continental shelf, representing the widening of the continental shelf at Cape Hatteras. In this case the separation point of the subtropical gyre oscillates between northern and southern separation positions, the southern position occurring at the point where the continental shelf widens. As the DWBC transport increases, the southern separation position is occupied more and more frequently, until we obtain a fairly steady separation for sufficiently large DWBC transports.

We can identify the changing separation behavior in our model with different dynamical regimes. Many other studies, e.g. Jiang *et al.* (1995), McCalpin and Haidvogel (1996), have investigated in detail the low frequency behavior of simple uniform depth, wind-driven models. In these experiments, low frequency behavior is moderated by changes in the wind forcing and the nonlinearity of the boundary current. In our experiments, changing the topography and the strength of the DWBC can also dramatically alter the time dependent behavior of the model. In some cases we find very low frequency variability, characterized by a separation point which changes abruptly after a period of several hundred days. Introduction of a DWBC into a primitive equation model was also found to produce a decadal timescale oscillation in the separation point by Spall (1996a,b). The mechanism for Spall's oscillation involved the periodic deflection of the DWBC into the recirculation gyres, which we do not observe in our model integrations. However, in common with Spall, we do find that the amplitude of the variability is reduced with large DWBC transports, although in our model we believe this is due to the separation locking on to the shelf widening point as described above.

b. Role of coastline geometry

The excess variability at the separation point in our experiments is most likely a consequence of the straight coastline in our idealized domain. In a nonrotating fluid, in the case of flow along a surface containing a salient edge, the separation is observed to always occur at the salient edge, with the flow separating tangentially to the upstream face (Batchelor, 1967). Stern and Whitehead (1990) showed that in a rotating fluid, separation occurs provided the coastline angle exceeds a critical value. The coastline at Cape Hatteras does possess a salient edge, and the Gulf Stream does indeed separate more or less tangentially. In contrast, in our experiments, the boundary current is forced to retroflect in order to separate. A similar retroflection is found as the Brazil Current and the East

Australia Current separate—both currents show much larger variability in the separation point than the Gulf Stream. In practice, variability may be further reduced because the Gulf Stream is shielded from the subpolar gyre, although this isolation of the two boundary currents does occur in our experiments with a strong DWBC.

In reality, the Gulf Stream does not separate from a vertical boundary. Prior to separation, the Gulf Stream approximately follows the 200 m isobath, in which the salient edge at Cape Hatteras is less pronounced. However, Stern (1998) pointed out that the isobaths converge near Cape Hatteras, and this may also lead to the Gulf Stream separating, where the separation is from a sloping bottom rather than a vertical side wall. Precisely how this result is modified by a DWBC will require further study.

c. Role of large-scale forcing

While we have emphasized the importance of local effects in explaining the absence of variability found in the Gulf Stream separation point, large-scale wind and buoyancy forcing must also play a role in the separation problem (Parsons, 1969; Nurser and Williams, 1990). In addition, Veronis (1973) pointed out that processes occurring in the eastern North Atlantic affect the separation of the Gulf Stream through the mass budget of the upper thermocline. These processes will include the northward transport into the Norwegian Sea, and also the transport into the Mediterranean.

More locally, Ezer and Mellor (1992) suggested that maintenance of a cyclonic northern recirculation gyre is important in obtaining the correct separation latitude. They achieved this in their model through buoyancy forcing, and a prescribed barotropic inflow along the continental shelf near Grand Banks. However, the presence of a northern recirculation gyre is the inevitable consequence of a Gulf Stream separating at Cape Hatteras, so cause and effect is not clear. The moderation of the lower layer recirculation by the topography shown in our experiments suggests that the topography may be important in influencing the northern recirculation gyre, and so aiding Gulf Stream separation in this way.

d. Implications for general circulation models

Ocean general circulation models generally produce a Gulf Stream which separates too far north. We have shown that the DWBC can lead to a southward shift in the separation. However, the excessive variability in our experiments suggests that an accurate representation of the coastline is also important to obtain a realistic simulation of the Gulf Stream separation.

Recent high resolution simulations of the North Atlantic at 1/10° (Smith *et al.,* 2000) and 1/12° resolution (Paiva *et al.,* 1999) do show a plausible Gulf Stream separation. However, in the foreseeable future, we will be unable to perform many long climate integrations at this resolution. Hence a clear understanding of the processes involved in Gulf Stream separation remains important, and will require further process studies such as the one we have described in this paper. The geostrophic vorticity model is an ideal tool for such studies.

Acknowledgments. This study is supported by the UK Natural Environment Research Council, GR3/10157, and in part by the UK Meteorological Office, met1b/2170. We are also very grateful to Alistair Adcroft (MIT) for providing us with the three-dimensional multigrid solver.

APPENDIX

a. Derivation of the Rossby wave equation

All variables are defined in Section 3. Following Allen *et al.* (1990), we rearrange the momentum equation (Eqs. 11 and 12) to obtain an expression for the full velocity, **u**, in each of the two layers, and substitute for **u** in the continuity equation (Eqs. 16 and 17). Defining $h_{gn} = 1/Q_{gn}$, this gives a Rossby wave equation:

$$\frac{\partial h_n}{\partial t} + \nabla \cdot \left\{ h_{gn} \left(\mathbf{k} \times \nabla B_{gn} - \mathbf{k} \times \mathscr{F}_n + \mathbf{k} \times \frac{\partial \mathbf{u}_{gn}}{\partial t} \right) \right\} = 0 \qquad n = 1, 2 \tag{27}$$

where $\mathscr{F}_n$ represents forcing and dissipation terms on the right-hand side of the momentum equation.

Employing geostrophic and hydrostatic balance, and noting that $\partial h_2/\partial t = \partial H/\partial t - \partial h_1/\partial t = -\partial h_1/\partial t$, this gives two inseparable equations for $\partial p/\partial t$ in the two layers:
Layer 1

$$\frac{1}{\rho_0 g'} \left(\frac{\partial p_1}{\partial t} - \frac{\partial p_2}{\partial t} \right) - \nabla \cdot \left(\frac{h_{g^1}}{\rho_0 f} \nabla \left(\frac{\partial p_1}{\partial t} \right) \right) = -\nabla \cdot (h_{g^1} (\mathbf{k} \times \nabla B_{g^1} - \mathbf{k} \times \mathscr{F}_1)) \tag{28}$$

Layer 2

$$-\frac{1}{\rho_0 g'} \left(\frac{\partial p_1}{\partial t} - \frac{\partial p_2}{\partial t} \right) - \nabla \cdot \left(\frac{h_{g^2}}{\rho_0 f} \nabla \left(\frac{\partial p_2}{\partial t} \right) \right) = -\nabla \cdot (h_{g^2} (\mathbf{k} \times \nabla B_{g^2} - \mathbf{k} \times \mathscr{F}_2)). \tag{29}$$

These two elliptic equations, together with the boundary conditions, can be inverted to obtain $\partial p/\partial t$ explicitly in each layer. This is done using a 3-d multigrid solver. Centered time differencing is used to update the pressure fields from these pressure tendencies, using a Robert-Asselin filter of 0.01. Diffusion and friction terms are lagged.

b. Model grid and finite differencing scheme

Our model grid is shown in Figure 16.

Putting $\mathbf{u} = \mathbf{u}' + \mathbf{u}^*$, where

$$h\mathbf{u}^* = h_g (\mathbf{k} \times \nabla B_g - \mathbf{k} \times \mathscr{F}) \tag{30}$$

and

$$h\mathbf{u}' = -\frac{h_g}{\rho_0 f} \nabla \left(\frac{\partial p}{\partial t} \right) \tag{31}$$

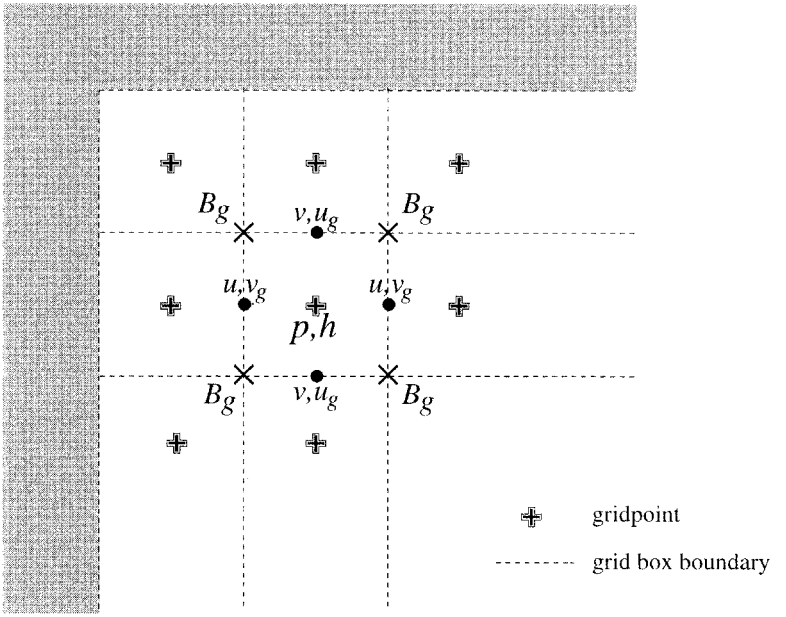

Figure 16. Model grid.

allows us to write Eqs. 16 and 17 in flux form:

$$\nabla \cdot (h\mathbf{u}') = \delta_x \left[-\frac{\overline{h_g^x}}{\rho_0 f} \delta_x \left(\frac{\partial p}{\partial t} \right) \right] + \delta_y \left[-\frac{\overline{h_g^y}}{\rho_0 f} \delta_y \left(\frac{\partial p}{\partial t} \right) \right] \tag{32}$$

$$\begin{aligned} \nabla \cdot (h\mathbf{u}^*) = {} & \delta_x \left[\overline{h_g^x} \left(-\delta_y B - K\nabla^4 v_g - r(z) v_g + s(y)(v_{g^0} - v_g) \right) \right] \\ & + \delta_y \left[\overline{h_g^y} \left(\delta_x B - \frac{\tau(z)}{\rho \overline{h^y}} + K\nabla^4 u_g + r(z) u_g - s(y)(u_{g^0} - u_g) \right) \right] \end{aligned} \tag{33}$$

where

$$\begin{aligned} r(z) &= 0 \qquad \text{in layer 1} \\ &= r \qquad \text{in layer 2} \end{aligned} \tag{34}$$

$$\begin{aligned} \tau(z) &= \tau_{sx} \qquad \text{in layer 1} \\ &= 0 \qquad \text{in layer 2} \end{aligned} \tag{35}$$

$$\delta_x \phi = \frac{1}{\Delta x} \left[\phi\left(x + \frac{\Delta x}{2} \right) - \phi\left(x - \frac{\Delta x}{2} \right) \right] \tag{36}$$

$$\overline{\phi^x} = \frac{1}{2}\left[\phi\left(x + \frac{\Delta x}{2}\right) + \phi\left(x - \frac{\Delta x}{2}\right)\right] \tag{37}$$

$$\nabla^2(\phi) = \delta_x^2 + \delta_y^2 \tag{38}$$

and similarly for δ_y and $\overline{\phi^y}$. At the model boundaries, hu' and hv' are set to zero, and hu^* and hv^* are set to zero unless there is a fixed inflow or outflow, when hu^* and hv^* are given by the prescribed transport into or out of the boundary.

REFERENCES

Allen, J. S., J. A. Barth and P. A. Newberger. 1990. On intermediate models for barotropic continental shelf and slope flow fields. Part III: Comparison of numerical model solutions. J. Phys. Oceanogr., *20,* 1949–1973.

Auer, S. J. 1987. Five-year climatological survey of the Gulf Stream and its associated rings. J. Geophys. Res., *92,* 11709–11726.

Baines, P. B. and R. L. Hughes. 1996. Western boundary current separation: inferences from a laboratory experiment. J. Phys. Oceanogr., *26,* 2576–2588.

Batchelor, G. K. 1967. An Introduction to Fluid Dynamics. Cambridge University Press, 615 pp.

Bell, M. J. 1999. Vortex stretching and bottom torques in the Bryan-Cox ocean circulation model. J. Geophys. Res., *104,* 23545–23563.

Berloff, P. and S. P. Meacham. 1998. The dynamics of a simple baroclinic model of the wind-driven circulation. J. Phys. Oceanogr., *28,* 361–388.

Bogden, P. S., R. E. Davis and R. Salmon. 1993. The North Atlantic circulation: Combining simplified dynamics with hydrographic data. J. Mar. Res., *51,* 1–52.

Bower, A. S. and H. D. Hunt. 2000. Lagrangian observations of the Deep Western Boundary Current in the North Atlantic Ocean. Part II: The Gulf Stream-Deep Western Boundary Current crossover. J. Phys. Oceanogr., *30,* 784–804.

Cessi, P., R. V. Condie and W. R. Young. 1990. Dissipative dynamics of western boundary currents. J. Mar. Res., *48,* 677–700.

Cloke, P. and M. J. P. Cullen. 1994. A semi-geostrophic ocean model with outcropping. Dyn. Atmos. Oceans, *21,* 23–48.

Dengg, J. 1993. The problem of Gulf Stream separation: a barotrophic approach. J. Phys. Oceanogr., *23,* 2182–2200.

Dengg, J., A. Beckmann and R. Gerdes. 1996. The Gulf Stream separation problem. The Warmwatersphere of the North Atlantic, W. Kraus, ed., Gebruder Borntrager, 446 pp.

Ezer, T. and G. L. Mellor. 1992. A numerical study of the variability and the separation of the Gulf Stream induced by surface atmospheric forcing and lateral boundary flows. J. Phys. Oceanogr., *22,* 660–682.

Greatbatch, R. J., A. F. Fanning, A. D. Goulding and S. Levitus. 1991. A diagnosis of interpental circulation changes in the North Atlantic. J. Geophys. Res., *96,* 22009–22023.

Haidvogel, D. B., J. C. McWilliams and P. R. Gent. 1992. Boundary current separation in a quasigeostrophic, eddy-resolving ocean circulation model. J. Phys. Oceanogr., *22,* 882–902.

Hogg, N. G. and H. Stommel. 1985. On the relationship between the deep circulation and the Gulf Stream. Deep-Sea Res., *32,* 1181–1193.

Hoskins, B. J. 1975. The geostrophic momentum approximation and the semigeostrophic equations. J. Atmos. Sci., *32,* 233–240.

Jiang, S., F. F. Jin and M. Ghil. 1995. Multiple equilibria, periodic, and aperiodic solutions in a wind-driven, double-gyre, shallow-water model. J. Phys. Oceanogr., *25,* 764–786.

Ladd, C. and L. Thompson. 1998. The influence of eddies and tracer transport in the abyssal ocean. J. Phys. Oceanogr., *28,* 1717–1738.

McCalpin, J. D. and D. B. Haidvogel. 1996. Phenomenology of the low-frequency variability in a reduced-gravity, quasigeostrophic double-gyre model. J. Phys. Oceanogr., *26,* 739–752.

Myers, P. G., A. F. Fanning and A. J. Weaver. 1996. JEBAR, bottom pressure torque, and Gulf Stream separation. J. Phys. Oceanogr., *26,* 671–682.

Nurser, G. A. J. and R. G. Williams. 1990. Cooling Parsons' model of the separated Gulf Stream. J. Phys. Oceanogr., *20,* 1974–1979.

Olson, D. B., G. P. Podesta, R. H. Evans and O. B. Brown. 1988. Temporal variations in the separation of the Brazil and Malvinas Currents. Deep-Sea Res., *35,* 1971–1990.

Özgökmen, T. M., E. P. Chassignet and A. M. Paiva. 1997. Impact of wind forcing, bottom topography and inertia on midlatitude jet separation in a quasigeostrophic model. J. Phys. Oceanogr., *27,* 2460–2476.

Paiva, A. M., J. T. Hargrove, E. P. Chassignet and R. Bleck. 1999. Turbulent behaviour of a fine mesh (1/12°) numerical simulation of the North Atlantic. J. Mar. Sys., *21,* 307–320.

Parsons, A. T. 1969. A two-layer model of Gulf Stream separation. J. Fluid Mech., *39,* 511–528.

Pedlosky, J. 1996. Ocean Circulation Theory, Springer-Verlag, 453 pp.

Pickart, R. S. and W. M. Smethie Jr. 1993. How does the deep western boundary current cross the Gulf Stream? J. Phys. Oceanogr., *23,* 2602–2616.

Pickart, R. S. and D. R. Watts. 1990. Deep western boundary current variability at Cape Hatteras. J. Mar. Res., *48,* 765–791.

Salmon, R. 1992. A two-layer Gulf Stream over a continental slope. J. Mar. Res., *50,* 341–365.

—— 1994. Generalized two-layer models of the ocean circulation. J. Mar. Res., *52,* 865–908.

Schär, C. and H. C. Davies. 1988. Quasigeostrophic stratified flow over isolated finite topography. Dyn. Atmos. Oceans, *11,* 287–306.

Smith, R. D., M. E. Maltrud, F. O. Bryan and M. W. Hecht. 2000. Numerical simulation of the North Atlantic Ocean at 1/10°. J. Phys. Oceanogr., *30* (in press).

Spall, M. A. 1996a. Dynamics of the Gulf Stream/Deep Western Boundary Current crossover. Part I: Entrainment and recirculation. J. Phys. Oceanogr., *26,* 2152–2168.

—— 1996b. Dynamics of the Gulf Stream/Deep Western Boundary Current crossover. Part II: low-frequency internal oscillations. J. Phys. Oceanogr., *26,* 2169–2182.

Stern, M. E. 1998. Separation of a density current from the bottom of a continental slope. J. Phys. Oceanogr., *28,* 2040–2049.

Stern, M. E. and J. A. Whitehead. 1990. Separation of a boundary jet in a rotating fluid. J. Fluid. Mech., *217,* 41–69.

Thompson, J. D. and W. J. Schmitz Jr. 1989. A limited-area model of the Gulf Stream: Design, initial experiments, and model-data intercomparison. J. Phys. Oceanogr., *19,* 791–814.

Thompson, L. 1995. The effect of continental rises on the wind-driven ocean circulation. J. Phys. Oceanogr., *25,* 1296–1316.

Veronis, G. 1973. Model of World Ocean Circulation: I. Wind-driven, two layer. J. Mar. Res., *31,* 228–288.

Received: *11 March, 1999;* revised: *3 January, 2000.*